A NEW METHOD FOR CALCULATING CONDUCTION RESPONSE FACTORS FOR MULTILAYER CONSTRUCTIONS BASED ON FREQUENCY–DOMAIN SPLINE INTERPOLATION (FDSI) AND ASYMPTOTIC ANALYSIS

Javier SANZA PÉREZ [a], Manuel ANDRÉS CHICOTE [a,b], Fernando VARELA DÍEZ [c], Eloy VELASCO GÓMEZ [a]

[a] University of Valladolid, School of Engineering, Department of Energy Engineering and Fluidmechanics. Paseo del Cauce n.59, 47011, Valladolid, Spain

[b] CARTIF Technology Center, Parque Tecnológico de Boecillo, 205, 47151 Boecillo, Valladolid, Spain

[c] Universidad Nacional de Educación a Distancia (UNED), School of Industrial Engineering, Department of Energy Engineering. Juan del Rosal n.12, 28040, Madrid, Spain

Abstract

Conduction heat transfer through building construction elements is one of the main components of space heating and cooling loads, and, thus, one of the key aspects when planning sustainable energy designs in the building sector. The Response Factors (RF) method sets the base for related dynamic calculations implemented by most well-known Building Energy Simulation (BES) software, and it represents a research topic of present interest. In this regard, this work introduces a new method for calculating conduction Response Factors in building multilayer constructions, based on the definition of an approximated wall model through Frequency–Domain Spline Interpolation (FDSI) and asymptotic analysis. Its conceptual development as well as first validations comparing with existing methods from previous literature are presented. Finally, as a result of applying a table-lookup approach and the possibility of pre-calculating most of the involved operations, an accurate, fast and easy-to-code algorithm is obtained, which constitutes a promising alternative to improve the current state-of-art calculation procedures.

Keywords: Building transient heat transfer, Thermal Response Factors, spline interpolation, frequency-domain, asymptotic analysis.

Nomenclature

General

a, b, c, d	coefficients of the piecewise polynomial approximation
A_k, B_k, C_k, D_k	transmission matrix elements of the k^{th} construction layer

A_T, B_T, C_T, D_T	transmission matrix elements of the total multilayer construction
c_p	specific heat capacity [$J \cdot kg^{-1} \cdot K^{-1}$]
E	Error estimate (%)
f_k	cubic spline approximation functions [$W \cdot m^{-2} \cdot K^{-1}$]
F[…]	Fourier transform
F^{-1}[…]	inverse Fourier transform
G	transfer function
h_k	amplitude of the intervals between frequency evaluation points (ω_k) [$rad \cdot s^{-1}$]
L	layer thickness [m]
j	complex variable
MFF	Modified Frequency Function [$W \cdot m^{-2} \cdot K^{-1}$]
q	heat flux [$W \cdot m^{-2}$]
R	thermal resistance [$m^2 \cdot K \cdot W^{-1}$]
r_k	slope of the MFFs at selected frequency evaluation points (ω_k)
s	independent variable in the Laplace domain
t	time [s]
T	temperature [C]
$\dot{T}$	first derivative of the temperature variable [$C \cdot s^{-1}$]
T_Δ	shaping function [-]
Δt	timestep [s]
U	wall’s thermal transmittance [$W \cdot m^{-2} \cdot K^{-1}$]
X_{RF}, Y_{RF}, Z_{RF}	internal, cross and external terms for the Response Factor method [$W \cdot m^{-2} \cdot K^{-1}$]
X_{CTF}, Y_{CTF}, Z_{CTF}	internal, cross and external terms for the CTF method [$W \cdot m^{-2} \cdot K^{-1}$]
y_k	Value of the MFFs at selected frequency evaluation points (ω_k) [$W \cdot m^{-2} \cdot K^{-1}$]

Greek symbols

α	thermal diffusivity [$m^2 \cdot s^{-1}$]
β_k	roots of the transfer function $B_T(s)$
λ	thermal conductivity [$W \cdot m^{-1} \cdot K^{-1}$]
ψ	amplitude of the frequency characteristic
Γ_k, φ_k	auxiliary terms for the recursive calculation of the spline coefficients

Φ	weighting coefficients of the previous heat fluxes in the CTF method [-]
ρ	material density [$kg \cdot m^{-3}$]
σ_k	second derivative of the MFFs at selected frequency evaluation points
ω	frequency [$rad \cdot s^{-1}$]

Subscripts

a, b, c, d	relative to the corresponding coefficients of the piecewise polynomial approximation
i, k	integer counts
A / P	asymptotic / polynomial
C / S	cosine / sine
H / T	head / tail
int / ext	internal / external
m	number of timesteps
n	total number of elements of a given vector or identifier of a given element into a Response Factor series (X, Y or Z)
N	total number of frequency points
X, Y, Z	relative to the corresponding term of the Response Factor method

Acronyms

BES	Building Energy Simulation
CTF	Conductive Transfer Functions
DRF	Direct Root Finding
FDR	Frequency-Domain Regression
FDM	Finite Difference Method
FDSI	Frequency-Domain Spline Interpolation
FEM	Finite Element Method
HVAC	Heating, Ventilating and Air Conditioning
RF	Response Factors
SSM	State-Space Method

Specific notation for FDSI method constants and integration factors

AF	Asymptotic function
k	constant (construction-dependent)

K integration factor (construction non-dependent) ([1],[2])

([1]) KAHC, KAHS, KATC, KATS, KPCa, KPCb, KPCc, KPCd, KPSa, KPSb, KPSc, KPSd are those 'integration factors' which can be interpreted according to the following criteria:

A/P: asymptotic/polynomial

H/T: head/tail

C/S: cosine/sine

a/b/c/d: associated to the corresponding spline coefficient

([2]) KATC0, KATC(+), KATS(+), KATC (-), KATS(-) are particular definitions of the integration factors to determine the tail asymptotic equivalents

1. Introduction

As energy and environmental sustainability in the building sector have become increasingly important in these days, Building Energy Simulation (BES) software has attained a fundamental role in the design of new constructions and the planning of energy retrofitting actions [1,2]. This software can estimate the amount of energy required to assure indoor thermal comfort conditions throughout the year (that is to say, space heating and cooling loads), which allows architects and engineers to better benefit from passive energy techniques and design more efficient HVAC systems and strategies. In this sense, among other capabilities, BES software involves methods to evaluate short-wave and long-wave radiative heat transfer, convective heat flows, one-dimensional heat conduction through multi-layered walls, as well as the dynamics of the energy facilities within the built environment.

In particular, the conduction heat transfer through building construction elements is one of the key components of space loads. Wang and Chen [3] present an exhaustive review of those methods available to determine its contribution. Despite the existence of numerical methods [4,5] and the so-called harmonic or periodic approaches [6,7], currently, the most widely used techniques are the Response Factors (RF) method and the Conductive Transfer Function (CTF) method, which set the base for the calculations implemented by well-known BES programs such as Energy-Plus [8] or TRNSYS [9]. These methods are generally considered to derive from the research conducted by Mitalas and Stephenson [10-12]

The Response Factors method calculates the heat flux at discrete times as a function of the previous temperatures on both sides of the construction (Eqs.1).

$$q_{ext}(i \cdot \Delta t) = \sum_{k=0}^{\infty} X_{RF}[k] \cdot T_{ext}[(i-k) \cdot \Delta t] - \sum_{k=0}^{\infty} Y_{RF}[k] \cdot T_{int}[(i-k) \cdot \Delta t] \quad Eq.1a$$

$$q_{int}(i \cdot \Delta t) = \sum_{k=0}^{\infty} Y_{RF}[k] \cdot T_{ext}[(i-k) \cdot \Delta t] - \sum_{k=0}^{\infty} Z_{RF}[k] \cdot T_{int}[(i-k) \cdot \Delta t] \quad Eq.1b$$

T_{int} and T_{ext} strictly are the internal and external surface temperatures. However, for general validation purposes, numerous case studies from literature often consider them to represent ambient temperatures including massless inner and outer layers with a thermal resistance value equivalent to that derived from the corresponding convective heat transfer coefficient (see Tables 5 and 7). The terms X[k], Y[k] and Z[k] for k ranging from zero to infinity are called response factors (RF). These factors tend to zero when k tend to infinity so, in practice, a finite number of them is accurate enough to describe the construction dynamics. However, the simulation of HVAC systems integrated in BES programs sometimes requires time-steps shorter than 1 hour to reproduce realistic control strategies and equipment time responses. In such situations, the required amount of RF to get good accuracy often becomes inconveniently large for computer implementation [3, 13].

The Conductive Transfer Function method (CTF) [12] reduces the number of terms needed to describe the construction dynamics. This method expresses the internal and external heat flux values at a given time in a more convenient form as a function of a finite number of previous temperatures and previous heat fluxes (see Eqs.2).

$$q_{ext}(i \cdot \Delta t) = \sum_{k=0}^{N} X_{CTF}[k] \cdot T_{ext}[(i-k) \cdot \Delta t] - \sum_{k=0}^{N} Y_{CTF}[k] \cdot T_{int}[(i-k) \cdot \Delta t] + \sum_{k=1}^{M} \Phi[k] \cdot q_{ext}[(i-k) \cdot \Delta t] \quad Eq.2a$$

$$q_{int}(i \cdot \Delta t) = \sum_{k=0}^{\infty} Y_{CTF}[k] \cdot T_{ext}[(i-k) \cdot \Delta t] - \sum_{k=0}^{\infty} Z_{CTF}[k] \cdot T_{int}[(i-k) \cdot \Delta t] + \sum_{k=1}^{M} \Phi[k] \cdot q_{int}[(i-k) \cdot \Delta t] \quad Eq.2b$$

The series of terms $X_{RF}[k]$, $Y_{RF}[k]$ and $Z_{RF}[k]$ for the Response Factor Method (RF) as well as $X_{CTF}[k]$, $Y_{CTF}[k]$ and $Z_{CTF}[k]$ for the Conductive Transfer Function Method (CTF), can be calculated by several procedures.

The use of Laplace transform methods is probably the most extended one. Briefly, these methods obtain the heat flux response of the construction to a temperature shaping function (typically a triangle of height one) in the frequency domain, and then apply the inverse Laplace transform to get the corresponding solution in the time domain. Eqs.3 show the expressions for the Response Factors, where $A_T(s)$, $B_T(s)$, $C_T(s)$ and $D_T(s)$ are the terms of the characteristic matrix of the construction (see section 2), while β_k are the poles of the transfer function $B_T(s)$.

$$X_{RF}(t) = t \cdot \left[\frac{D_T(s)}{B_T(s)}\right]_{s=0} + \frac{d}{ds}\left[\frac{D_T(s)}{B_T(s)}\right]_{s=0} + \sum_{k=1}^{\infty} \frac{1}{{\beta_k}^2} \cdot \left[\frac{D_T(s)}{B_T(s)}\right]_{s=0} \cdot e^{-\beta_k \cdot t} \quad Eq.3a$$

$$Y_{RF}(t) = t \cdot \left[\frac{1}{B_T(s)}\right]_{s=0} + \frac{d}{ds}\left[\frac{1}{B_T(s)}\right]_{s=0} + \sum_{k=1}^{\infty} \frac{1}{{\beta_k}^2} \cdot \left[\frac{1}{B_T(s)}\right]_{s=0} \cdot e^{-\beta_k \cdot t} \quad Eq. 3b$$

$$Z_{RF}(t) = t \cdot \left[\frac{A_T(s)}{B_T(s)}\right]_{s=0} + \frac{d}{ds}\left[\frac{A_T(s)}{B_T(s)}\right]_{s=0} + \sum_{k=1}^{\infty} \frac{1}{{\beta_k}^2} \cdot \left[\frac{A_T(s)}{B_T(s)}\right]_{s=0} \cdot e^{-\beta_k \cdot t} \quad Eq. 3c$$

This approach was first developed by Stephenson and Mitalas [10-12] and later improved by other authors [13, 14] in order to avoid pole skipping and enhance calculation efficiency. These methods are often referred as Direct Root-Finding (DRF) methods, as the inversion process (based on the residue theorem) involves iterative root finding, which is computationally expensive. In addition, the number of poles is infinite, so one must settle for a limited number of them. Varela et al. [15] proposed the Direct Numerical Integration (DNI) of the inversion formula as a viable option.

Moreover, other alternatives not based on the Laplace transform have been developed to obtain the RF or CTF coefficients. Davies [16] evaluated them using elementary time domain solutions for wall heat flow. Similarly, State-Space Methods (SSM) [17] are also based on a time-domain formulation. As shown in Figure 1, a temperature node is set for each construction layer. Then, a numeric algorithm (Finite Element Method - FEM, or Finite Differences Method - FDM) is applied to obtain the terms of the matrices A, B, C and D of the equivalent space-state model. Once the terms of these matrices are calculated, the coefficients of the conduction transfer function (CTF) can be deduced by Leverrier's algorithm [18].

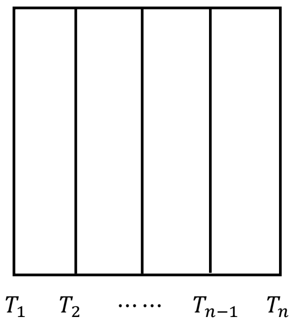

$$\begin{bmatrix} \dot{T}_1 \\ \dot{T}_2 \\ \vdots \\ \dot{T}_n \end{bmatrix} = A \cdot \begin{bmatrix} T_1 \\ T_2 \\ \vdots \\ T_n \end{bmatrix} + B \cdot \begin{bmatrix} T_{int} \\ T_{ext} \end{bmatrix} \quad Eq. 4a$$

$$\begin{bmatrix} q_{int} \\ q_{ext} \end{bmatrix} = C \cdot \begin{bmatrix} T_1 \\ T_2 \\ \vdots \\ T_n \end{bmatrix} + D \cdot \begin{bmatrix} T_{int} \\ T_{ext} \end{bmatrix} \quad Eq. 4b$$

Figure 1. General approach of the space-state methods

Seem et al. [19] demonstrated that this approach can also be used to calculate transfer functions for walls that require two-dimensional models, which could be applied to overcome the limitations of the one-dimensional approach when dealing with hollow blocks or relevant thermal bridge effects into wall constructions. In this sense, Kossecka et al. [20] also described a method to derive conduction z-transfer function coefficients from response factors for 3D wall assemblies. Moreover, Kosny et al. [21] contributed to the accuracy improvement in whole building thermal modeling tools, through the definition of an 'equivalent wall' concept and the proposal of additional thermal structure factors to account for building envelope components containing high thermal mass and/or 2D and 3D heat transfer effects.

However, state-space formulations for multi-dimensional heat conduction problems often rely on linear models with high-order matrices involving important computation times. Gao et al. [22] proposed a solution based on the application of model reduction techniques to decrease computation costs with no significant accuracy losses.

Returning to the Response Factor method for 1D transient heat transfer, another more recent methodology consists of the Frequency-Domain Regression (FDR) methods developed by Wang et al. [3, 23-26]. They set out a general transfer function whose parameters are estimated by a regression algorithm (Eq. 5). Starting from several frequency evaluations of the construction dynamics, these methods find the set of coefficients that minimize the quadratic error between those evaluations and the ones given by the approximate model.

$$G(s) = \frac{\beta_0 + \beta_1 \cdot s + \beta_2 \cdot s^2 + \cdots + \beta_{r-1} \cdot s^{r-1} + \beta_r \cdot s^r}{1 + \alpha_1 \cdot s + \alpha_2 \cdot s^2 + \cdots + \alpha_{m-1} \cdot s^{m-1} + \alpha_m \cdot s^m} \quad Eq. 5$$

It is a fast and accurate method. In addition, it allows a direct calculation of the coefficients for the CTF method instead of the sequence of response factors (RF).

Finally, it should be remarked that research on this field is of present interest, what can be supported by additional improved or innovative approaches contributed in recent years [27-34].

Along these lines, this work introduces a new method for calculating conduction response factors (RF) of building multilayer constructions. It is based on the definition of an approximated wall model through Frequency–Domain Spline Interpolation (FDSI) and asymptotic analysis. First, temperature evolutions are expressed as sums of harmonics by means of Fourier transform methods. Then, the FDSI model is applied to obtain the heat flux solution in the frequency domain. Nevertheless, the particular definition of such wall model enables to rearrange the Fourier transform inversion integrals so that each response factor is obtained as the sum of several simple terms. In addition, those terms depending on the construction thermo-physical properties can be separated and pre-calculated, making it possible to use an efficient table-lookup approach. Therefore, the FDSI method provides an accurate, fast and easy-to-code alternative to the current RF calculation methodologies.

2. Frequency response in multilayer constructions

Given the Laplace model of a construction, it is easy to evaluate the gain and the phase shift associated to each frequency. For a particular layer (k), its mathematical expression is the following [3]:

$$\begin{bmatrix} T_{ext} \\ q_{ext} \end{bmatrix} = \begin{bmatrix} A_k(s) & B_k(s) \\ C_k(s) & D_k(s) \end{bmatrix} \cdot \begin{bmatrix} T_{int} \\ q_{int} \end{bmatrix} \xrightarrow{s=j\omega} \begin{bmatrix} T_{ext} \\ q_{ext} \end{bmatrix} = \begin{bmatrix} A_k(j\omega) & B_k(j\omega) \\ C_k(j\omega) & D_k(j\omega) \end{bmatrix} \cdot \begin{bmatrix} T_{int} \\ q_{int} \end{bmatrix} \quad Eq. 6$$

$$\begin{bmatrix} A_k(j\omega) & B_k(j\omega) \\ C_k(j\omega) & D_k(j\omega) \end{bmatrix} = \begin{bmatrix} cosh\left(L_k \cdot \sqrt{\frac{j\omega}{\alpha_k}}\right) & \frac{sinh\left(L_k \cdot \sqrt{\frac{j\omega}{\alpha_k}}\right)}{\lambda_k \cdot \sqrt{\frac{j\omega}{\alpha_k}}} \\ \lambda_k \cdot \sqrt{\frac{j\omega}{\alpha_k}} \cdot sinh\left(L_k \cdot \sqrt{\frac{j\omega}{\alpha_k}}\right) & cosh\left(L_k \cdot \sqrt{\frac{j\omega}{\alpha_k}}\right) \end{bmatrix} \qquad Eq.7$$

Numeric evaluation of the matrix above for each frequency yields four complex numbers that describe the gain and phase shift of the layer thermal response associated to these frequencies. Besides, the characteristic matrix of the whole construction can be expressed as the product of the matrices for each individual layer:

$$\begin{bmatrix} A_T(j\omega) & B_T(j\omega) \\ C_T(j\omega) & D_T(j\omega) \end{bmatrix} = \begin{bmatrix} A_1(j\omega) & B_1(j\omega) \\ C_1(j\omega) & D_1(j\omega) \end{bmatrix} \cdot \begin{bmatrix} A_2(j\omega) & B_2(j\omega) \\ C_2(j\omega) & D_2(j\omega) \end{bmatrix} \cdots \begin{bmatrix} A_{n-1}(j\omega) & B_{n-1}(j\omega) \\ C_{n-1}(j\omega) & D_{n-1}(j\omega) \end{bmatrix} \cdot \begin{bmatrix} A_n(j\omega) & B_n(j\omega) \\ C_n(j\omega) & D_n(j\omega) \end{bmatrix} \qquad Eq.8$$

If heat fluxes are written down as a function of temperatures, the following formulation (Eq.9) is obtained.

$$\begin{bmatrix} q_{int} \\ q_{ext} \end{bmatrix} = \begin{bmatrix} \frac{D_T(j\omega)}{B_T(j\omega)} & -\frac{1}{B_T(j\omega)} \\ \frac{1}{B_T(j\omega)} & -\frac{A_T(j\omega)}{B_T(j\omega)} \end{bmatrix} \cdot \begin{bmatrix} T_{ext} \\ T_{int} \end{bmatrix} = \begin{bmatrix} X(\omega) & -Y(\omega) \\ Y(\omega) & -Z(\omega) \end{bmatrix} \cdot \begin{bmatrix} T_{ext} \\ T_{int} \end{bmatrix} \qquad Eq.9$$

Therefore:

$$X(\omega) = \frac{D_T(j\omega)}{B_T(j\omega)}; \quad Y(\omega) = \frac{1}{B_T(j\omega)}; \quad Z(\omega) = \frac{A_T(j\omega)}{B_T(j\omega)} \qquad Eqs.10$$

3. Description of the Frequency-Domain Spline Interpolation (FDSI) algorithm

The basic idea of the FDSI method is to split the temperature evolution into a sum of harmonics using the Fourier transform. Then, by means of an approximated model for the construction, the gain and phase shift for each frequency are calculated. Finally, this method gets the heat fluxes in time domain using the inverse Fourier transform.

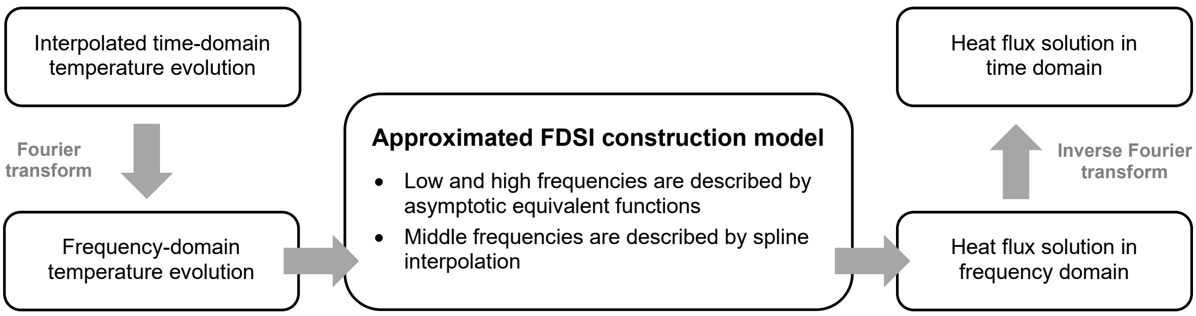

Figure 2. Block diagram for the FDSI fundamental conception

In order to simplify this method, the temperature evolution between sampling points is often considered as linear. This is a reasonable assumption when such evolution is sufficiently slow compared to the time interval between these points, but not when there are abrupt temperature changes.

Considering this hypothesis, the interpolated time-domain function can be split into a set of triangular pulses, as it is represented in Figure 3.

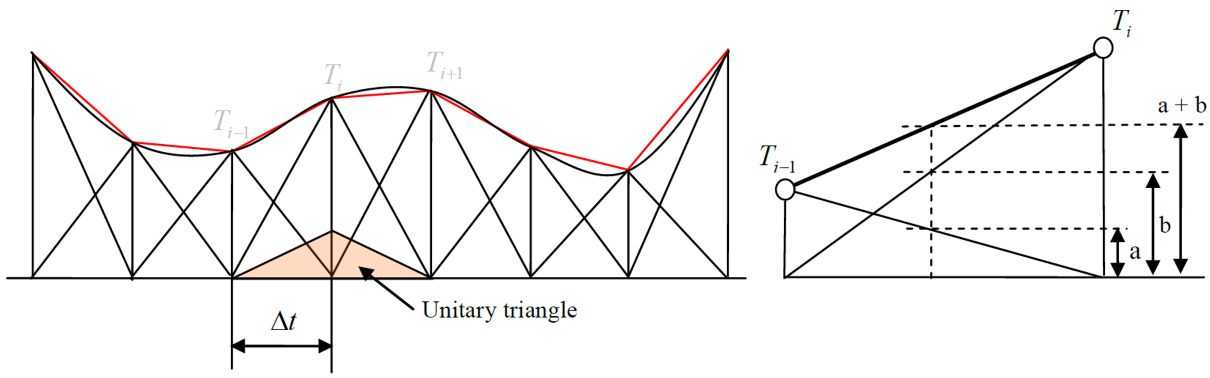

Figure 3. Breakdown of a linearly interpolated temperature evolution into unitary triangles

Therefore, the temperature function (for both the external or the internal temperature variables) can be expressed as the sum of a set of scaled and shifted unitary triangles (T_Δ) which constitute the so-called 'shaping function'. Figure 4 describes in detail the characteristics of such function.

$$T(t) = \sum_{k=-\infty}^{m} T(k \cdot \Delta t) \cdot T_\Delta(t - k \cdot \Delta t) \quad with \quad m \cdot \Delta t \geq t \quad Eq. 11$$

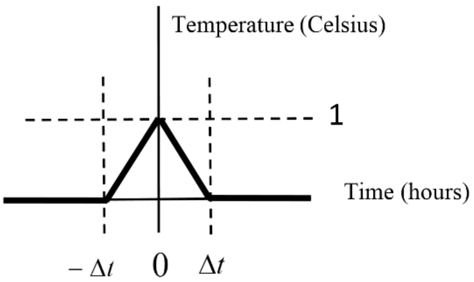

$$T_\Delta(t) = \begin{cases} 0 & if\ t < -\Delta t \\ \dfrac{t + \Delta t}{\Delta t} & if\ t \in [-\Delta t, 0] \\ \dfrac{-t + \Delta t}{\Delta t} & if\ t \in [0, \Delta t] \\ 0 & if\ t > \Delta t \end{cases} \quad Eq. 12$$

Figure 4. Description of a triangular shaping function

Shaping functions might also adopt expressions other than triangular, thus describing different types of interpolation [34]. In this case, starting from the temperature as a linear combination of shaping functions, the Fourier transforms yields an equivalent sum of harmonics. For the external temperature evolution this can be expressed through the equation Eq.13a.

$$T_{ext}(\omega) = F[T_{ext}(t)] = F\left[\sum_{k=-\infty}^{m} T_{ext}(k \cdot \Delta t) \cdot T_\Delta(t - k \cdot \Delta t)\right] = \sum_{k=-\infty}^{m} T_{ext}(k \cdot \Delta t) \cdot F[T_\Delta(t - k \cdot \Delta t)]$$

$$= \sum_{k=-\infty}^{m} T_{ext}(k \cdot \Delta t) \cdot e^{-k \cdot \Delta t \cdot j\omega} \cdot F[T_\Delta(t)] \quad with \quad m \cdot \Delta t \geq t \quad Eq. 13a$$

Similarly, Eq.13b can be derived for the internal temperature evolution:

$$T_{int}(\omega) = F[T_{int}(t)] = \sum_{k=-\infty}^{m} T_{int}(k \cdot \Delta t) \cdot e^{-k \cdot \Delta t \cdot j\omega} \cdot F[T_{\Delta}(t)] \qquad with \quad m \cdot \Delta t \geq t \qquad Eq.13b$$

According to this formulation, the heat flux solutions in the frequency domain are obtained as follows:

$$q_{ext}(\omega) = X(\omega) \cdot T_{ext}(\omega) - Y(\omega) \cdot T_{int}(\omega) =$$

$$= X(\omega) \cdot \sum_{k=-\infty}^{m} T_{ext}(k \cdot \Delta t) \cdot e^{-k \cdot \Delta t \cdot j\omega} \cdot F[T_{\Delta}(t)] - Y(\omega) \cdot \sum_{k=-\infty}^{m} T_{int}(k \cdot \Delta t) \cdot e^{-k \cdot \Delta t \cdot j\omega} \cdot F[T_{\Delta}(t)] \quad Eq.14a$$

$$q_{int}(\omega) = Y(\omega) \cdot T_{ext}(\omega) - Z(\omega) \cdot T_{int}(\omega) =$$

$$= Y(\omega) \cdot \sum_{k=-\infty}^{m} T_{ext}(k \cdot \Delta t) \cdot e^{-k \cdot \Delta t \cdot j\omega} \cdot F[T_{\Delta}(t)] - Z(\omega) \cdot \sum_{k=-\infty}^{m} T_{int}(k \cdot \Delta t) \cdot e^{-k \cdot \Delta t \cdot j\omega} \cdot F[T_{\Delta}(t)] \quad Eq.14b$$

At this point, heat fluxes in time domain can be calculated via the inverse Fourier transform.

$$q_{ext}(t) = F^{-1}[q_{ext}(\omega)]; \quad q_{int}(t) = F^{-1}[q_{int}(\omega)] \quad Eq.15$$

$$q_{ext}(t) = \sum_{k=-\infty}^{m} T_{ext}(k \cdot \Delta t) \cdot F^{-1}\left[X(\omega) \cdot e^{-k \cdot \Delta t \cdot j\omega} \cdot F[T_{\Delta}(t)]\right] - \sum_{k=-\infty}^{m} T_{int}(k \cdot \Delta t) \cdot F^{-1}\left[Y(\omega) \cdot e^{-k \cdot \Delta t \cdot j\omega} \cdot F[T_{\Delta}(t)]\right] =$$

$$= \sum_{k=-\infty}^{m} T_{ext}(k \cdot \Delta t) \cdot F^{-1}\big[X(\omega) \cdot F[T_{\Delta}(t)]\big](t - k \cdot \Delta t) - \sum_{k=-\infty}^{m} T_{int}(k \cdot \Delta t) \cdot F^{-1}\big[Y(\omega) \cdot F[T_{\Delta}(t)]\big](t - k \cdot \Delta t) \quad Eq.16a$$

$$q_{int}(t) = \sum_{k=-\infty}^{m} T_{ext}(k \cdot \Delta t) \cdot F^{-1}\big[Y(\omega) \cdot F[T_{\Delta}(t)]\big](t - k \cdot \Delta t) - \sum_{k=-\infty}^{m} T_{int}(k \cdot \Delta t) \cdot F^{-1}\big[Z(\omega) \cdot F[T_{\Delta}(t)]\big](t - k \cdot \Delta t) \; Eq.16b$$

In the formulation above, the following expression yields the response factors by conveniently substituting in Eq.17 the term RF (Response Factor) by each corresponding series of factors (X, Y or Z).

$$RF(t) = F^{-1}\big[RF(\omega) \cdot F[T_{\Delta}(t)]\big] =$$

$$= \frac{1}{\sqrt{2\pi}} \int_{-\infty}^{\infty} |RF(\omega)| \cdot e^{j \cdot arg[RF(\omega)]} \cdot F[T_{\Delta}(t)] \cdot e^{j\omega t}\, d\omega = \frac{1}{\sqrt{2\pi}} \int_{-\infty}^{\infty} |RF(\omega)| \cdot e^{(\omega t + arg[RF(\omega)]) \cdot j} \cdot F[T_{\Delta}(t)]\, d\omega \qquad Eq.17$$

If the shaping function is even (as it happens to be when linear interpolation is applied to the temperature evolution) the above integral can be rewritten in a much simpler way.

$$RF(t) = F^{-1}\big[RF(\omega) \cdot F[T_{\Delta}(t)]\big] = \sqrt{\frac{2}{\pi}} \int_{-\infty}^{\infty} |RF(\omega)| \cdot F[T_{\Delta}(t)] \cdot cos(\omega t + arg[RF(\omega)]) \cdot d\omega \qquad Eq.18$$

$$RF(t) = F^{-1}\big[RF(\omega) \cdot F[T_{\Delta}(t)]\big] =$$

$$= \sqrt{\frac{2}{\pi}} \int_{-\infty}^{\infty} |RF(\omega)| \cdot F[T_{\Delta}(t)] \cdot [cos(\omega t) \cdot cos(arg[RF(\omega)]) - sin(\omega t) \cdot sin(arg[RF(\omega)])] \cdot d\omega \qquad Eq.19$$

These expressions could be solved analytically if the exact phase shift and the amplitude gain functions were used for each frequency. However, this becomes exceedingly complex, so X(ω), Y(ω) and Z(ω) will be substituted by an approximate description inferred from a limited number of frequency evaluations.

With this idea in perspective, it results useful to group all the terms that depend on the construction into separate functions which, from now on, will be called “Modified Frequency Functions” or MFFs. Eqs.20 develop this approach for each response factor.

$$X_{RF}(t)=\sqrt{\frac{2}{\pi}}\int_{-\infty}^{\infty} MFF_{XC}(\omega)\cdot F[T_\Delta(t)]\cdot cos(\omega t)\cdot d\omega-\sqrt{\frac{2}{\pi}}\int_{-\infty}^{\infty} MFF_{XS}(\omega)\cdot F[T_\Delta(t)]\cdot sin(\omega t)\cdot d\omega \qquad Eq.20a$$

$$Y_{RF}(t)=\sqrt{\frac{2}{\pi}}\int_{-\infty}^{\infty} MFF_{YC}(\omega)\cdot F[T_\Delta(t)]\cdot cos(\omega t)\cdot d\omega-\sqrt{\frac{2}{\pi}}\int_{-\infty}^{\infty} MFF_{YS}(\omega)\cdot F[T_\Delta(t)]\cdot sin(\omega t)\cdot d\omega \qquad Eq.20b$$

$$Z_{RF}(t)=\sqrt{\frac{2}{\pi}}\int_{-\infty}^{\infty} MFF_{ZC}(\omega)\cdot F[T_\Delta(t)]\cdot cos(\omega t)\cdot d\omega-\sqrt{\frac{2}{\pi}}\int_{-\infty}^{\infty} MFF_{ZS}(\omega)\cdot F[T_\Delta(t)]\cdot sin(\omega t)\cdot d\omega \qquad Eq.20c$$

where:

$$MFF_{XC}(\omega)=|X(\omega)|\cdot cos\big[arg[X(\omega)]\big] \qquad Eq.21a$$

$$MFF_{XS}(\omega)=|X(\omega)|\cdot sin\big[arg[X(\omega)]\big] \qquad Eq.21b$$

$$MFF_{YC}(\omega)=|Y(\omega)|\cdot cos\big[arg[Y(\omega)]\big] \qquad Eq.21c$$

$$MFF_{YS}(\omega)=|Y(\omega)|\cdot sin\big[arg[Y(\omega)]\big] \qquad Eq.21d$$

$$MFF_{ZC}(\omega)=|Z(\omega)|\cdot cos\big[arg[Z(\omega)]\big] \qquad Eq.21e$$

$$MFF_{ZS}(\omega)=|Z(\omega)|\cdot sin\big[arg[Z(\omega)]\big] \qquad Eq.21f$$

If MFFs are replaced by third order piecewise polynomials inside a given frequency range [ω_1, ω_2] and by asymptotic functions outside this range, the following general expression (Eq.22) for the X response factor is obtained.

$$X_{RF}(n\cdot\Delta t)=\sqrt{\frac{2}{\pi}}\cdot\left\{\begin{array}{c}\displaystyle\int_{0}^{\omega_1}[k_{XHC1}\cdot AF_{HC1}(\omega)+k_{XHC2}\cdot AF_{HC2}(\omega)]\cdot F[T_\Delta(t)]\cdot cos(\omega\cdot n\cdot\Delta t)\cdot d\omega+\\ \displaystyle+\sum_{k=1}^{N-1}\left[\int_{\omega_i}^{\omega_{i+1}}\left(a_{XC(k)}\cdot\omega^3+b_{XC(k)}\cdot\omega^2+c_{XC(k)}\cdot\omega+d_{XC(k)}\right)\cdot F[T_\Delta(t)]\cdot cos(\omega\cdot n\cdot\Delta t)\cdot d\omega\right]+\\ \displaystyle+\int_{\omega_N}^{\infty}[k_{XTC1}\cdot AF_{TC1}(\omega)+k_{XTC2}\cdot AF_{TC2}(\omega)]\cdot F[T_\Delta(t)]\cdot cos(\omega\cdot n\cdot\Delta t)\cdot d\omega-\\ \displaystyle-\int_{0}^{\omega_1}[k_{XHS1}\cdot AF_{HS1}(\omega)+k_{XHS2}\cdot AF_{HS2}(\omega)]\cdot F[T_\Delta(t)]\cdot sin(\omega\cdot n\cdot\Delta t)\cdot d\omega-\\ \displaystyle-\sum_{k=1}^{N-1}\left[\int_{\omega_i}^{\omega_{i+1}}\left(a_{XS(k)}\cdot\omega^3+b_{XS(k)}\cdot\omega^2+c_{XS(k)}\cdot\omega+d_{XS(k)}\right)\cdot F[T_\Delta(t)]\cdot sin(\omega\cdot n\cdot\Delta t)\cdot d\omega\right]-\\ \displaystyle-\int_{0}^{\omega_1}[k_{XTS1}\cdot AF_{TS1}(\omega)+k_{XTS2}\cdot AF_{TS2}(\omega)]\cdot F[T_\Delta(t)]\cdot sin(\omega\cdot n\cdot\Delta t)\cdot d\omega\end{array}\right\} \quad Eq.22$$

Eq.22 can be adapted in the same way for Y and Z response factors, but they are not presented here for the sake of simplicity.

It should be noted that the asymptotic approximations of the MFFs out of the selected frequency range have been defined through the following general expression:

$$MFF(\omega) \approx k_1 \cdot AF_1(\omega) + k_2 \cdot AF_2(\omega) \qquad Eq.23$$

where k_1 and k_2 are constants, and $AF_1(\omega)$ and $AF_2(\omega)$ are functions that describe the asymptotic behavior of the MFFs along the 'head' $[0, \omega_1]$ and 'tail' $[\omega_2, \infty)$ frequency intervals. Sections 4 and 6 describe in detail the particular expressions of these constants and functions that should be applied on the calculation of each response factor (X, Y, or Z) along the head or tail intervals.

Finally, Eq.22 can be rearranged so that each response factor is simply obtained as the sum of several terms. Each addend will be the product of a factor that depends on the construction characteristics (lowercase constants) by another factor that can be pre-calculated (uppercase constants). Next, Eq.24 shows the expression of the X response factor as an example, but, again, similar expressions can be derived in the same way for Y and Z factors.

$$X_{RF}(n \cdot \Delta t) =$$

$$= \sqrt{\frac{2}{\pi}} \cdot \left\{ \begin{array}{c} k_{XHC1} \cdot KAHC1_n + k_{XHC2} \cdot KAHC2_n + \sum_{k=1}^{N-1} \left[a_{XC(k)} \cdot KPCa_{n,k} + b_{XC(k)} \cdot KPCb_{n,k} + c_{XC(k)} \cdot KPCc_{n,k} + d_{XC(k)} \cdot KPCd_{n,k} \right] + \\ + k_{XHS1} \cdot KAHS1_n + k_{XHS2} \cdot KAHS2_n - k_{XTC1} \cdot KATC1_n - k_{XTC2} \cdot KATC2_n - \\ - \sum_{k=1}^{N-1} \left[a_{XS(k)} \cdot KPSa_{n,k} + b_{XS(k)} \cdot KPSb_{n,k} + c_{XS(k)} \cdot KPSc_{n,k} + d_{XS(k)} \cdot KPSd_{n,k} \right] - k_{XTS1} \cdot KATS1_n - k_{XTS2} \cdot KATS2_n \end{array} \right\} Eq.24$$

The uppercase constants (which from now on will be named as "integration factors") do not depend on the construction and can be obtained analytically. Therefore, they need to be calculated only once and then can be embedded as part of the FDSI main algorithm developed to obtain the response factors. Section 4 presents the detailed expressions of these integration factors.

On the other hand, the constants that depend on the construction characteristics are the spline coefficients for each frequency interval and the constants associated to the definition of the asymptotic equivalents. All of them can be easily calculated by evaluating the MFFs at several frequency points, as it is described in sections 5 and 6.

In conclusion, once all the integrals are pre-calculated and stored inside a large table, the operations to be performed by the FDSI method are reduced to the following:

- Evaluation of the Modified Frequency Functions (MFFs) at several frequency points, logarithmically spaced.
- Spline interpolation of the MFFs.
- Calculation of the coefficients associated to the asymptotic equivalents.
- Sum of the products of the spline coefficients by the integration terms to calculate each response factor.

4. Generation of the integration factors

In order to generate the table of terms to be embedded within the method as pre-calculated factors, it is necessary to solve a certain number of definite integrals. As it has been previously mentioned, there are two types of integration factors, which can be referred as polynomial and asymptotic integration factors. The polynomial factors are those derived from the piecewise polynomial interpolation that approximate MFFs at middle frequencies. The asymptotic factors derive from the definition of equivalent asymptotic functions that approximate MFFs at high and low frequencies.

4.1. Integration factors for the spline coefficients that approximate MFFs at middle frequencies.

Table 1 gathers the integration factors that multiply the spline coefficients at each frequency interval (see Eq.24). There are 8·(k-1) terms of this kind for each response factor, being k the number of frequency points where the MFFs are evaluated.

Table 1: Integration factors for the spline interpolation

Cosine factors	Sine factors
$KPCa_{n,k} = \int_{\omega(k-1)}^{\omega(k)} \omega^3 \cdot F[T_\Delta(t)] \cdot cos(\omega \cdot n \cdot \Delta t) \cdot d\omega$	$KPSa_{n,k} = \int_{\omega(k-1)}^{\omega(k)} \omega^3 \cdot F[T_\Delta(t)] \cdot sin(\omega \cdot n \cdot \Delta t) \cdot d\omega$
$KPCb_{n,k} = \int_{\omega(k-1)}^{\omega(k)} \omega^2 \cdot F[T_\Delta(t)] \cdot cos(\omega \cdot n \cdot \Delta t) \cdot d\omega$	$KPSb_{n,k} = \int_{\omega(k-1)}^{\omega(k)} \omega^2 \cdot F[T_\Delta(t)] \cdot sin(\omega \cdot n \cdot \Delta t) \cdot d\omega$
$KPCc_{n,k} = \int_{\omega(k-1)}^{\omega(k)} \omega \cdot F[T_\Delta(t)] \cdot cos(\omega \cdot n \cdot \Delta t) \cdot d\omega$	$KPSc_{n,k} = \int_{\omega(k-1)}^{\omega(k)} \omega \cdot F[T_\Delta(t)] \cdot sin(\omega \cdot n \cdot \Delta t) \cdot d\omega$
$KPCd_{n,k} = \int_{\omega(k-1)}^{\omega(k)} F[T_\Delta(t)] \cdot cos(\omega \cdot n \cdot \Delta t) \cdot d\omega$	$KPSd_{n,k} = \int_{\omega(k-1)}^{\omega(k)} F[T_\Delta(t)] \cdot sin(\omega \cdot n \cdot \Delta t) \cdot d\omega$

(*) $F[T_\Delta(t)] = \frac{1-cos(\omega \cdot \Delta t)}{\omega^2 \cdot \Delta t}$ *for linear interpolation.*

4.2. Integration factors for the asymptotic functions that approximate MFFs at low and high frequencies.

So far, eight different terms of this kind have been proposed in a general description of the asymptotic equivalents (see Eq.24): KAHC1, KAHC2, KAHS1 and KAHS2 for the low-frequency or head interval, and KATC1, KATC2, KATS1 and KATS2 for the high-frequency or tail interval.

The low-frequency asymptotic behavior can be described by the same four head functions for any series of response factors (X, Y and Z) and in any particular case. However, that is not the case for the tail terms. Fortunately, it can be proved that proper combinations of only 5 different integration factors are needed to characterize this high-frequency behavior in any situation. From now on, these tail integration factors are named as KATC0, KATC(+), KATC(-), KATS(+) and KATS(-). The relation between them and the general asymptotic tail terms showed in Eq.24 depends on the response factor being calculated, as well as on the existence or inexistence of a zero-inertia outermost or innermost wall layer.

The rearrangement of these integration factors is a consequence of the particular form of the MFFs. Further considerations for practical implementation of the FDSI method are given in Appendix A. Nevertheless, a complete derivation of the asymptotic analysis that leads to these terms would be too long to be presented on this paper and has been intentionally omitted here.

Next, Table 2 compiles the aforementioned integration factors, which multiply the construction-dependent constants associated to the definition of the asymptotic equivalents. In conclusion, one can observe that 8 integration asymptotic factors need to be calculated.

Table 2: Integration factors for the approximate asymptotic functions

Head asymptotic equivalents (low frequency)	**Tail asymptotic equivalents (high frequency)**
$KAHC1_n = \int_0^{\omega_1} F[T_\Delta(t)] \cdot cos(\omega \cdot n \cdot \Delta t) \cdot d\omega$	$KATC0_n = \int_{\omega_N}^{\infty} F[T_\Delta(t)] \cdot cos(\omega \cdot n \cdot \Delta t) \cdot d\omega$
$KAHC2_n = \int_0^{\omega_1} \omega \cdot (e^{\omega} - 1) \cdot F[T_\Delta(t)] \cdot cos(\omega \cdot n \cdot \Delta t) \cdot d\omega$	$KATC(+)_n = \int_{\omega_N}^{\infty} \omega^{0.5} \cdot F[T_\Delta(t)] \cdot cos(\omega \cdot n \cdot \Delta t) \cdot d\omega$
$KAHS1_n = \int_0^{\omega_1} (e^{\omega} - 1) \cdot F[T_\Delta(t)] \cdot sin(\omega \cdot n \cdot \Delta t) \cdot d\omega$	$KATS(+)_n = \int_{\omega_N}^{\infty} \omega^{0.5} \cdot F[T_\Delta(t)] \cdot sin(\omega \cdot n \cdot \Delta t) \cdot d\omega$
$KAHS2_n = 0$	$KATC(-)_n = \int_{\omega_N}^{\infty} \omega^{-0.5} \cdot F[T_\Delta(t)] \cdot cos(\omega \cdot n \cdot \Delta t) \cdot d\omega$
	$KATS(-)_n = \int_{\omega_N}^{\infty} \omega^{-0.5} \cdot F[T_\Delta(t)] \cdot sin(\omega \cdot n \cdot \Delta t) \cdot d\omega$

Finally, it should be noted that both types of integration factors must be stored into a large table. However, this is not an issue for modern computers in order to handle the FDSI method easily. For example, if the number of intervals between frequency evaluations (k-1) is 1024 and the number of response factors is 300, the total number of terms to be handled is the following:

$$m = 8 \cdot (k-1) \cdot n + 8 \cdot n \approx 8 \cdot 1024 \cdot 300 = 2457600 \text{ terms} \qquad \text{Eq.25}$$

If each element of the table is stored as a double precision floating point number (8 bytes), the total size of the table would be 19660800 bytes, that is to say, 18.75 MB. Modern computers can easily hold tables this size and larger in RAM memory. Similar results can be obtained with less frequency evaluations and, therefore, with a smaller factor table, as it will be shown in the validation section.

5. Spline interpolation of the Modified Frequency Functions (MFFs)

An approximate model for the Modified Frequency Functions (MFFs) at middle frequencies can be performed by piecewise polynomials (see Figure 5). The target is to have an ensemble of simple expressions that describes the MFFs between the frequency evaluation points with sufficient accuracy.

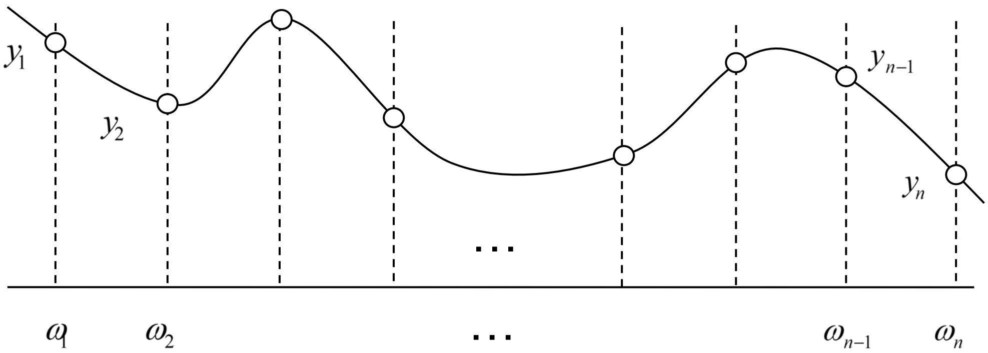

Figure 5. Piecewise polynomial interpolation approach

In order to achieve this goal, the FDSI method turns to cubic splines, as they are suitable for continuous smooth functions. Starting from a set of n evaluations of the MFFs at logarithmically-spaced frequencies within the selected range [ω_1, ω_n], (n-1) cubic polynomials (f_k) are defined, and their corresponding coefficients a_k, b_k, c_k and d_k (Eq.26) are calculated.

$$f_k(\omega) = a_k \cdot \omega^3 + b_k \cdot \omega^2 + c_k \cdot \omega + d_k \qquad Eq. 26$$

This calculation can be performed by a linear-time complexity algorithm. Particularly, based on the application of not-a-knot boundary conditions, Appendix B presents a detailed description of the recursive calculation procedure to get the spline coefficients in global coordinates.

6. Asymptotic analysis of the Modified Frequency Functions (MFFs)

Spline interpolation is able to reproduce with excellent precision the so-called Modified Frequency Functions (MFFs) inside a given frequency range. However, outside this range the error becomes unacceptably large since splines are not suitable for extrapolation. Luckily, when the frequency is sufficiently low or sufficiently high, it is possible to replace the complex dynamics of the construction by simple asymptotic equivalents that can be easily integrated into the method.

Given a general one-layer construction, the corresponding asymptotic equivalents can be expressed as follows in Table 3.

Table 3: Expression of the asymptotic equivalents for a one-layer construction

Term	Exact Modified Frequency Functions (one-layer construction)	Approximated functions
X	$\|X(\omega)\|\cdot cos\varphi(\omega)=\left\|\frac{D_T(j\omega)}{B_T(j\omega)}\right\|\cdot cos\left(arg\left(\frac{D_T(j\omega)}{B_T(j\omega)}\right)\right)=$ $=\left\|\lambda\cdot\sqrt{\frac{j\omega}{\alpha}}\cdot coth\left(L\cdot\sqrt{\frac{j\omega}{\alpha}}\right)\right\|\cdot cos\left(arg\left[\lambda\cdot\sqrt{\frac{j\omega}{\alpha}}\cdot coth\left(L\cdot\sqrt{\frac{j\omega}{\alpha}}\right)\right]\right)$	At high frequencies $\|X(\omega)\|\cdot cos\varphi(\omega)\approx\frac{\lambda}{\sqrt{2\alpha}}\cdot\omega^{0.5}$ At low frequencies $\|X(\omega)\|\cdot cos\varphi(\omega)\approx\frac{\lambda}{L}+\frac{\lambda\cdot L^3\cdot\omega\cdot(e^{\omega}-1)}{45\cdot\alpha^2}$
	$\|X(\omega)\|\cdot sin\varphi(\omega)=\left\|\frac{D_T(j\omega)}{B_T(j\omega)}\right\|\cdot sin\left(arg\left(\frac{D_T(j\omega)}{B_T(j\omega)}\right)\right)=$ $=\left\|\lambda\cdot\sqrt{\frac{j\omega}{\alpha}}\cdot coth\left(L\cdot\sqrt{\frac{j\omega}{\alpha}}\right)\right\|\cdot sin\left(arg\left[\lambda\cdot\sqrt{\frac{j\omega}{\alpha}}\cdot coth\left(L\cdot\sqrt{\frac{j\omega}{\alpha}}\right)\right]\right)$	At high frequencies $\|X(\omega)\|\cdot sin\varphi(\omega)\approx\frac{\lambda}{\sqrt{2\alpha}}\cdot\omega^{0.5}$ At low frequencies $\|X(\omega)\|\cdot sin\varphi(\omega)\approx\frac{\lambda\cdot L\cdot(e^{\omega}-1)}{3\alpha}$
Y	$\|Y(\omega)\|\cdot cos\varphi(\omega)=\left\|\frac{1}{B_T(j\omega)}\right\|\cdot cos\left(arg\left(\frac{1}{B_T(j\omega)}\right)\right)=$ $=\left\|\frac{\lambda\cdot\sqrt{\frac{j\omega}{\alpha}}}{sinh\left(L\cdot\sqrt{\frac{j\omega}{\alpha}}\right)}\right\|\cdot cos\left(arg\left[\frac{\lambda\cdot\sqrt{\frac{j\omega}{\alpha}}}{sinh\left(L\cdot\sqrt{\frac{j\omega}{\alpha}}\right)}\right]\right)$	At high frequencies $\|Y(\omega)\|\cdot cos\varphi(\omega)\approx 0$ At low frequencies $\|Y(\omega)\|\cdot cos\varphi(\omega)\approx\frac{\lambda}{L}+\frac{7k\cdot L^3\cdot\omega\cdot(e^{\omega}-1)}{360\cdot\alpha^2}$
	$\|Y(\omega)\|\cdot sin\varphi(\omega)=\left\|\frac{1}{B_T(j\omega)}\right\|\cdot sin\left(arg\left(\frac{1}{B_T(j\omega)}\right)\right)=$ $=\left\|\frac{\lambda\cdot\sqrt{\frac{j\omega}{\alpha}}}{sinh\left(L\cdot\sqrt{\frac{j\omega}{\alpha}}\right)}\right\|\cdot sin\left(arg\left[\frac{\lambda\cdot\sqrt{\frac{j\omega}{\alpha}}}{sinh\left(L\cdot\sqrt{\frac{j\omega}{\alpha}}\right)}\right]\right)$	At high frequencies $\|Y(\omega)\|\cdot sin\varphi(\omega)\approx 0$ At low frequencies $\|Y(\omega)\|\cdot sin\varphi(\omega)\approx\frac{\lambda\cdot L\cdot(e^{\omega}-1)}{6\alpha}$
Z	$\|Z(\omega)\|\cdot cos\varphi(\omega)=\left\|-\frac{A_T(j\omega)}{B_T(j\omega)}\right\|\cdot cos\left(arg\left(-\frac{A_T(j\omega)}{B_T(j\omega)}\right)\right)=$ $=\left\|-\lambda\cdot\sqrt{\frac{j\omega}{\alpha}}\cdot coth\left(L\cdot\sqrt{\frac{j\omega}{\alpha}}\right)\right\|\cdot cos\left(arg\left[-\lambda\cdot\sqrt{\frac{j\omega}{\alpha}}\cdot coth\left(L\cdot\sqrt{\frac{j\omega}{\alpha}}\right)\right]\right)$	At high frequencies $\|Z(\omega)\|\cdot cos\varphi(\omega)\approx-\frac{\lambda}{\sqrt{2\alpha}}\cdot\omega^{0.5}$ At low frequencies $\|Z(\omega)\|\cdot cos\varphi(\omega)\approx-\frac{\lambda}{L}-\frac{\lambda\cdot L^3\cdot\omega\cdot(e^{\omega}-1)}{45\cdot\alpha^2}$
	$\|Z(\omega)\|\cdot sin\varphi(\omega)=\left\|-\frac{A_T(j\omega)}{B_T(j\omega)}\right\|\cdot sin\left(arg\left(-\frac{A_T(j\omega)}{B_T(j\omega)}\right)\right)=$ $=\left\|-\lambda\cdot\sqrt{\frac{j\omega}{\alpha}}\cdot coth\left(L\cdot\sqrt{\frac{j\omega}{\alpha}}\right)\right\|\cdot sin\left(arg\left[-\lambda\cdot\sqrt{\frac{j\omega}{\alpha}}\cdot coth\left(L\cdot\sqrt{\frac{j\omega}{\alpha}}\right)\right]\right)$	At high frequencies $\|Z(\omega)\|\cdot sin\varphi(\omega)\approx-\frac{\lambda}{\sqrt{2\alpha}}\cdot\omega^{0.5}$ At low frequencies $\|Z(\omega)\|\cdot sin\varphi(\omega)\approx-\frac{\lambda\cdot L\cdot(e^{\omega}-1)}{3\alpha}$

When the construction is made from more than one layer, approximate functions are similar to the ones already shown in Table 3. They can be expressed, as well, in terms of several constants that depend on the properties of the layers. However, it is more practical to estimate these constants by evaluating the Modified Frequency Functions at the ends of the frequency vector used for spline interpolation; that is to say, at ω_1 for the asymptotic heads and ω_2 for the asymptotic tails.

A particular case arises again when the innermost or the outermost layer in the construction has zero density or zero thermal capacity, which is a reasonable approximation when thermal diffusivity is high enough. This assumption implies a change in the asymptotic functions, as shown in Table 4.

Table 4: Expression of the asymptotic equivalents for a multilayer construction considering zero-inertia cases

Functions for response	Approximate functions

factor calculation		High frequency			Low frequency
		Outermost layer without thermal inertia	Innermost layer without thermal inertia	All layers have thermal inertia	
X	$\lvert X(\omega)\rvert \cdot cos\big(arg(\lvert X(\omega)\rvert)\big)$	$\frac{\lambda_1}{L_1} - k_{XTC2} \cdot \omega^{-0.5}$ $\left(k_{XTC1} = \frac{\lambda_1}{L_1}\right)$	$k_{XTC2} \cdot \omega^{0.5}$ $(k_{XTC1} = 0)$	$k_{XTC2} \cdot \omega^{0.5}$ $(k_{XTC1} = 0)$	$\frac{1}{\sum_{i=1}^{n} \frac{L_i}{\lambda_i}} + \lambda_{XHC2} \cdot \omega \cdot (e^{\omega} - 1)$ $\left(k_{XHC1} = \frac{1}{\sum_{i=1}^{n} \frac{L_i}{\lambda_i}}\right)$
	$\lvert X(\omega)\rvert \cdot sin\big(arg(\lvert X(\omega)\rvert)\big)$	$k_{XTS2} \cdot \omega^{-0.5}$ $(k_{XTS1} = 0)$	$k_{XTS2} \cdot \omega^{0.5}$ $(k_{XTS1} = 0)$	$k_{XTS2} \cdot \omega^{0.5}$ $(k_{XTS1} = 0)$	$k_{XHS2} \cdot (e^{\omega} - 1)$ $(k_{XHS1} = 0)$
Y	$\lvert Y(\omega)\rvert \cdot cos\big(arg(\lvert Y(\omega)\rvert)\big)$	0	0	0	$\frac{1}{\sum_{i=1}^{n} \frac{L_i}{\lambda_i}} + k_{YHC2} \cdot \omega \cdot (e^{\omega} - 1)$ $\left(k_{YHC1} = \frac{1}{\sum_{i=1}^{n} \frac{L_i}{\lambda_i}}\right)$
	$\lvert Y(\omega)\rvert \cdot sin\big(arg(\lvert Y(\omega)\rvert)\big)$	0	0	0	$k_{YHS2} \cdot (e^{\omega} - 1)$ $(k_{YHS1} = 0)$
Z	$\lvert Z(\omega)\rvert \cdot cos\big(arg(\lvert Z(\omega)\rvert)\big)$	$k_{ZTC2} \cdot \omega^{0.5}$ $(k_{ZTC1} = 0)$	$\frac{\lambda_N}{L_N} - k_{ZTC2} \cdot \omega^{-0.5}$ $\left(k_{ZTC1} = \frac{\lambda_N}{L_N}\right)$	$k_{ZTC2} \cdot \omega^{0.5}$ $(k_{ZTC1} = 0)$	$-\frac{1}{\sum_{i=1}^{n} \frac{L_i}{\lambda_i}} + k_{ZHC2} \cdot \omega \cdot (e^{\omega} - 1)$ $\left(k_{ZHC1} = -\frac{1}{\sum_{i=1}^{n} \frac{L_i}{\lambda_i}}\right)$
	$\lvert Z(\omega)\rvert \cdot sin\big(arg(\lvert Z(\omega)\rvert)\big)$	$k_{ZTS2} \cdot \omega^{0.5}$ $(k_{ZTS1} = 0)$	$k_{ZTS2} \cdot \omega^{-0.5}$ $(k_{ZTS1} = 0)$	$k_{ZTS2} \cdot \omega^{0.5}$ $(k_{ZTS1} = 0)$	$k_{ZHS2} \cdot (e^{\omega} - 1)$ $(k_{zHS1} = 0)$

Once the constants k_{XTC1}, k_{XTC2}, k_{XTS2}, k_{XHC1}, k_{XHC2}, k_{XHS2}, k_{YHC1}, k_{YHC2}, k_{YHS2}, k_{ZTC1}, k_{ZTC2}, k_{ZTS2}, k_{ZHC1}, k_{ZHC2} and k_{ZHS2} are calculated, an accurate mathematical characterization of the MFFs for both low and high frequencies is completed, which combined with the spline model for intermediate frequencies yields a good approximation for the dynamics of the construction.

7. Complexity considerations and validation analyses

7.1. Algorithm complexity

The FDSI algorithm has a linear-time complexity. This means that increasing the number of response factors to be calculated (for instance in order to get accurate results with improved time resolution), multiplies the number of operations by the same scale factor.

This particular feature makes the FDSI method extremely fast compared to most of the previous alternatives. There is no need to solve systems of linear equations, to apply iterative pole finding or to use finite element algorithms, what would involve quadratic-time or even greater complexity and make the method much slower.

7.2. Validations

For the purpose of validation, the present FDSI method was tested in two different case studies, and the obtained results were compared with published data derived from previous existing methods. These case studies consist of two multilayered walls of different thermal inertia that have already served as test cases for other authors. Both are described in detail below.

Moreover, it should be noted that different criteria have been used for the comparison of the obtained results. In first place stationary thermal trasmittance (U-value) can be used as a checking parameter in the calculation of thermal response factors, as the sum of the infinite series of response factors for a given construction has to be equal to its U-value. Therefore, an error estimate can be expressed through Eq.27.

$$E_U(\%) = \left|\frac{U - \sum_{i=1}^{\infty} RF_i}{U}\right| \cdot 100 \qquad Eq.27$$

However, obtaining low values for this estimate is a necessary but not sufficient condition. That is to say, it does not guarantee itself the accuracy of the method, but having high E_U values always involves lack of it. Then, this estimate is presented for the studied test cases as a first premise, but also further validations are provided.

7.2.1. Case study I

The physical characteristics of the first test wall are presented in Table 5. It was chosen by Ouyang and Haghighat [17] to demonstrate the application of their SSM approach and then, it has been used by other authors to compare their own results, which derive from 3 other different methods, namely, DRF [35], FDR [3] and DNI [15].

Table 5: Detailed wall description of case study I

Description	L (mm)	λ (W·m^{-1}K^{-1})	ρ (kg·m^{-3})	c_p (J·kg^{-1}K^{-1})	R (m^2·K·W^{-1})
Outside surface film					0.0500
Concrete	89	1.73	2235	1106	0.0514
Insulation	127	0.0744	24	992	1.7070
Concrete	89	1.73	2235	1106	0.0514
Inside surface film					0.16

Table 6 compiles the first 20 cross (Y) response factors obtained by those methods (these data are extracted from [15]) and adds the corresponding results from the present FDSI approach. It can be observed that the accuracy of the FDSI results is comparable to that of the methodologies used so far.

Particularly, considering the reference of the FDR method as the most exact among them [15], the FDSI and the DNI alternatives clearly represent better approximations. Indeed, for this case study, it is noticeable that all the calculated response factors are identical for the FDSI and the DNI methods (at least considering the precision used in Table 6), when, however, they are based on completely different conceptual approaches.

Table 6: Comparison of thermal response factors for case study I obtained with different calculation methods

	FDR	SSM	DRF	DNI	FDSI
0	0.00001521	0.00001771	0.00001549	0.00001531	0.00001531
1	0.00163441	0.00164078	0.00164541	0.00163463	0.00163463
2	0.00849218	0.00852682	0.00852884	0.00849216	0.00849216
3	0.01600825	0.01606351	0.01605804	0.01600833	0.01600833
4	0.02127237	0.02132861	0.02132482	0.02127245	0.02127245
5	0.02453370	0.02458189	0.02458376	0.02453375	0.02453375
6	0.02630043	0.02634117	0.02634535	0.02630044	0.02630044
7	0.02697839	0.02701426	0.02701681	0.02697837	0.02697837
8	0.02687682	0.02690951	0.02690827	0.02687681	0.02687681
9	0.02622975	0.02625774	0.02625429	0.02622975	0.02622975
10	0.02521328	0.02523350	0.02523131	0.02521329	0.02521329
11	0.02395904	0.02397017	0.02397118	0.02395907	0.02395907
12	0.02256462	0.02256861	0.02257155	0.02256466	0.02256466
13	0.02110158	0.02110207	0.02110402	0.02110163	0.02110163
14	0.01962166	0.01962103	0.01962030	0.01962172	0.01962172
15	0.01816159	0.01815949	0.01815708	0.01816165	0.01816165
16	0.01674674	0.01674130	0.01673967	0.01674679	0.01674679
17	0.01539396	0.01538425	0.01538486	0.01539401	0.01539401
18	0.01411377	0.01410104	0.01410310	0.01411382	0.01411382
19	0.01291201	0.01289871	0.01290017	0.01291206	0.01291206

The twenty RF from Table 6 have been shown for comparison purposes, but it can be proved that they are insufficient to provide a complete representation of the transient thermal response of the selected wall. Actually, Table 7 presents the error estimate (E_U) when considering different number of thermal response factors calculated by the FDSI method.

Table 7: Error estimate E_U for the wall's response factors of case studies I and II calculated by the FDSI method

	Case study I Ouyang and Haghighat's wall	Case study II Chen's heavyweight wall

Number of RF (N)	$\sum_{i=1}^{N} RF_i$	E_U (%)	$\sum_{i=1}^{N} RF_i$	E_U (%)
20	0,3681307	25,642%	0,1846084	76,380%
50	0,4888178	1,265%	0,5783250	26,006%
100	0,4950393	0,008%	0,7491220	4,153%
150	0,4950788	0,000%	0,7763976	0,663%
200			0,7807529	0,106%
300			0,7815595	0,003%
Actual U-value	0,4950791		0,7815806	

As expected, the error is drastically reduced when considering a higher number of response factors, proving an adequate fulfilment of the U-value premise. Particularly, for Case study I, 100 calculated factors provide an error lower than 0.01%.

7.2.2. Case study II

Table 8 reports the physical properties of the second test construction selected for validation. It consists of a heavyweight wall widely used in China and proposed by Chen et al. [36] to demonstrate the application of a verification methodology for transient heat flow calculations in multilayered walls. Moreover, results derived from the DNI method [15] are also available in literature for this wall, what justifies the present choice.

Table 8: Detailed wall description of case study II

Description	L (mm)	λ ($W \cdot m^{-1} K^{-1}$)	ρ ($kg \cdot m^{-3}$)	c_p ($J \cdot kg^{-1} K^{-1}$)	R ($m^2 \cdot K \cdot W^{-1}$)
Outside surface film					0.0538
Common brick	370	0.814	1800	879	
Foam concrete	100	0.209	600	837	
Wood wool board	25	0.163	400	2093	
Stucco	20	0.814	1600	837	
Inside surface film					0.1147

In the first place, Table 7 should be referred again to check that the U-value premise is also fulfilled for Case study II. Indeed, the error estimate can be reduced to negligible values (lower than 0.005 %) when considering a properly high number of RF. However, in this case, approximately 300 factors are needed to get the aforementioned error values. This is consistent with the heavyweight characteristics of the present wall. Note that the number of response factors that are required to correctly model a given construction depends on its physical properties (which determine its time constant), as well as on the considered timestep.

In the second place, results obtained through the FDSI method have been compared with literature values according to the verification procedure developed in [36]. This methodology proposes the comparison of the theoretical frequency characteristics of the wall (obtained from its transmission matrix) with the dynamic behavior data derived from the calculated RF. This can be done visually by representing a Bode diagram with the amplitude and phase lag of the wall's thermal response. As an example, Figure 6 shows the theoretical and calculated characteristics of cross heat conduction for Case study II considering 144 factors.

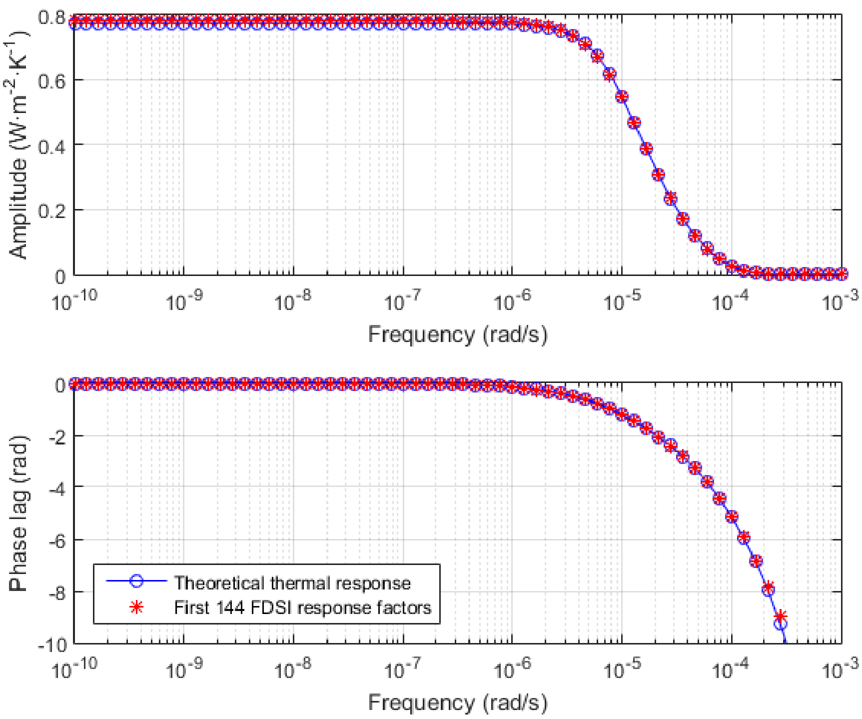

Figure 6. Comparison between the theoretical frequency response of the heavyweight wall (case study II) and that obtained from the calculated response factors with the FDSI method

It can be observed that both frequency characteristics are almost indistinguishable, what is also generally reported in literature for other test cases and calculation methods [3, 25, 36]. For this reason, the use of the following error estimate (Eq.28) was proposed and recommended [36].

$$E_\psi = \frac{1}{U}\sqrt{\frac{1}{N}\sum_{k=1}^{N}\left[\psi(\omega_k) - \tilde{\psi}(\omega_k)\right]^2} \cdot 100 \qquad Eq.28$$

According to this criterion, results from the FDSI, DNI and FDR methods are compared in Table 9. The first 72, 96, 120 and 144 cross (Y) factors were considered. Data from the existing methods were extracted from [15].

Table 9: Compared accuracy for FDSI, DNI and FDR methods for 'Case study II' wall.

Number of RF	72	96	120	144
E_ψ_FDSI (%)	9.15	3.76	1.55	0.64
E_ψ_DNI (%)	8.92	3.66	1.50	0.62
E_ψ_FDR (%)	9.12	3.74	1.54	0.63

It can be seen that the obtained errors for the FDSI method, despite being slightly higher, are very close to those of the DNI and the FDR method. As pointed out in [15], the latter, by definition, minimizes the present error estimate E_ψ, so the observed small differences prove a very interesting behavior of the FDSI method.

7.3. Accuracy dependence on the number of frequency points

Figure 7 shows an estimation of the absolute difference between the actual U-value and the sum of 300 calculated X response factors as a function of the number of frequency points used by the FDSI method when applied to 'Case study I'. Similar results can be obtained for Y and Z response factor series.

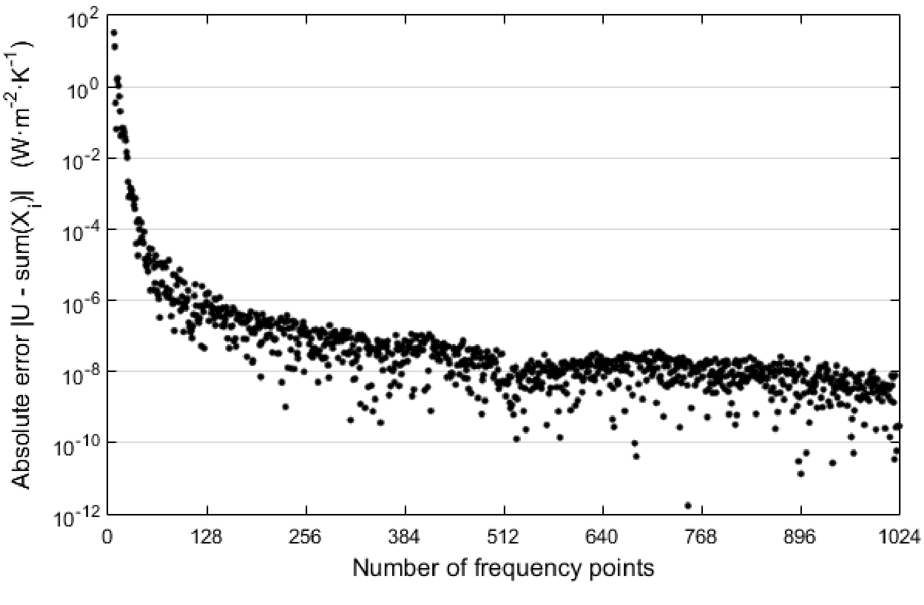

Figure 7. Influence of the number of frequency points on the method's accuracy

As expected, Figure 7 reveals that the accuracy of the FDSI method improves as the number of frequency points becomes larger, because the MFFs are better estimated. However, once the mathematical approximation is good enough, there is no use in increasing the number of interpolation points. With 512 frequency evaluations and a sufficient number of factors, the absolute error falls easily under 10^{-8}. Better estimates could be obtained by widening the frequency range or by calculating more response factors. Nevertheless, here the conceptual development and first validations of the FDSI method are presented, but further work needs to be done in this sense in the future.

Moreover, it should be noted that data in Figure 7 come from an indirect calculation procedure that provides approximated results. Only the pre-calculated integration factors for the case with 1024 frequency points were actually determined. For the other frequency sampling cases, the corresponding pre-calculated constants required by the FDSI method were estimated by a grouping routine. This aspect explains the scattering of the plot shown in Figure 7 and suggests not considering those exceptional accuracy values associated to certain singular frequencies.

8. Conclusions

This work has introduced a new method for the calculation of conduction response factors in multilayer constructions, based on frequency–domain spline interpolation (FDSI) and asymptotic analysis. Its conceptual development as well as first validations comparing with existing methods from previous literature have been presented.

The FDSI method enables the calculation of thermal response factors with great accuracy and speed, which constitutes a promising alternative to improve those procedures implemented in Building Energy Simulation programs so far. Particularly, it can make BES tools able to efficiently calculate with small timesteps (1-5 min) which is of special interest in energy simulations combining buildings and HVAC systems that often have much shorter time responses. In order to run simulations with small timesteps (keeping the level of accuracy), the only requirement is to calculate more response factors, but thanks to the lookup table approach most of the involved calculations will be done only once and stored, so the ‘small timestep’ condition will not increase a lot the computational effort and make such simulations affordable.

In summary, the following features characterize the new proposed method:

- Precision: As integration factors can be pre-calculated beforehand with excellent precision, error depends only on the number of frequency evaluations, the number of factors and the width of the frequency range. With 512 frequency evaluations and a sufficient number of factors, the estimate for this variable falls easily under 10^{-8}.

- Speed: This algorithm has linear-time complexity, which makes it extremely fast compared to other methods. There is no need to solve linear systems, iterative pole finding or the use of finite element algorithms. It just requires N frequency evaluations, the calculation of spline coefficients and 8·N multiplications for each response factor.
- Stability: FDSI method is inherently stable. Convergence is always guaranteed because there are no iterative numeric algorithms involved.

As a drawback, this method requires several megabyte of RAM to store the pre-calculated integration factors. However, since modern computers are able to handle up to several gigabytes of main memory, this is not a relevant issue.

Acknowledgements

This paper is based upon work supported by the Spanish Government through the national research project '*OPtimisation of design and integrated operation of Thermo-Active Building Systems (TABS) and LOW-energy sources for Mediterranean climate, OPTABSLOW*' (Ref.: ENE2014-58990-R)

References

[1] J.L.M. Hensen, R. Lamberts. Building Performance Simulation for Design and Operation. Routledge (2011) ISBN: 9780415474146.

[2] J.A. Clarke. Energy Simulation in Building Design. 2nd edition. Routledge (2001) ISBN: 9780750650823.

[3] Shengwei Wang, Youming Chen. Transient heat flow calculation for multilayer constructions using a frequency-domain regression method. Building and Environment, 38 (2003) 45-61.

[4] S. V. Patankar. Numerical Heat Transfer and Fluid Flow. McGraw-Hill Book Company (1980) ISBN: 0070487405

[5] C. Luo, B. Moghtaderi, H. Sugo, A. Page. A new stable finite volume method for predicting thermal performance of a whole building. Building and Environment, 43 (2008) 37-43.

[6] Jeffrey D. Spitler, Daniel E. Fisher, Curtis O. Pedersen. The Radiant Time Series Cooling Load Calculation Procedure. ASHRAE Transactions, 103 (2) (1997) 503-515.

[7] Fernando Varela, Francisco J. Rey, Eloy Velasco, Santiago Aroca. The harmonic method: A new procedure to obtain wall periodic cross response factors. International Journal of Thermal Sciences, 58 (2012) 20-28

[8] EnergyPlus™ Version 8.5 Documentation. Engineering Reference. U.S. Department of Energy (2016)

[9] TRNSYS 17. A TRaNsient System Simulation Program. Volume 5. Multizone Building modeling with Type 56 and TRNBuild. Solar Energy Laboratory, University of Wisconsin-Madison (2012)

[10] D.G. Stephenson, G.P. Mitalas. Cooling load calculations by thermal response factor method. ASHRAE Transactions, 73 (1) (1967) III1.1–III.1.7.

[11] G.P. Mitalas, D.G. Stephenson. Room thermal response factors. ASHRAE Transactions 73 (1) (1967) 2.1–2.10.

[12] D.G. Stephenson, G.P. Mitalas. Calculation of heat conduction transfer functions for multilayer slabs. ASHRAE Transactions, 77 (2) (1971) 117–126.

[13] Ismael R. Maestre, Paloma R. Cubillas, Luis Pérez-Lombard. Transient heat conduction in multi-layer walls: An efficient strategy for Laplace's method, Energy and Buildings, 42 (2010) 541-546.

[14] Douglas C. Hittle, Richard Bishop. An improved root-finding procedure for use in calculating transient heat flow through multilayered slabs. International Journal of Heat and Mass Transfer, 26 (11) (1983) 1685-1693.

[15] Fernando Varela, Santiago Aroca, Cristina González, Antonio Rovira. A direct numerical integration (DNI) method to obtain wall thermal response factors. Energy and Buildings, 81 (2014) 363-370.

[16] M. G. Davies. Wall Transient Heat Flow using Time-Domain Analysis. Building and Environment, 32 (5) (1997) 427-446.

[17] K. Ouyang, F. Haghighat. A procedure for calculating thermal response factors of multilayer walls state-space method. Building and Environment, 26 (2) (1991) 173–177.

[18] Bing Zheng, Guorong Wang. Leverrier's algorithm and Cayley-Hamilton theorem for 2D system. Applied Mathematics and Computation, 160 (2005) 725-738.

[19] J.E. Seem, S.A. Klein, W.A. Beckman, J.W. Michelle, Transfer Functions for Efficient Calculation of Multidimensional Transient Heat Transfer, Journal of Heat Transfer, 111 (1) (1989) 5-12

[20] E. Kossecka, J. Kosny, Three-dimensional conduction z-transfer function coefficients determined from the response factors, Energy and Buildings, 37 (4) (2005) 301-310

[21] J. Kosny, E. Kossecka, Multi-dimensional heat transfer through complex building envelope assemblies in hourly energy simulation programs, Energy and Buildings, 34 (5) (2002), 445-454.
[22] Y. Gao, J.J. Roux, C. Teodosiu, L.H. Zhao. Reduced linear state model of hollow blocks walls, validation using hot box measurements. Energy and Buildings 36 (2004) 1107–1115.
[23] Youming Chen, Shengwei Wang. Frequency-domain regression method for estimating CTF models of building multilayer constructions. Applied Mathematical Modelling, 25 (2001) 579-590
[24] Youming Chen, Shengwei Wang. A new procedure for calculating periodic response factors based on frequency domain regression method. International Journal of Thermal Sciences, 44 (2005) 382-392.
[25] Xinhua Xu, Shengwei Wang, Youming Chen. An improvement to frequency-domain regression method for calculating conduction transfer functions of building walls. Applied Thermal Engineering, 28 (2008) 661-667.
[26] Jinbo Wang, Shengwei Wang, Xinhua Xu, Youming Chen. Short time step heat flow calculation of building constructions based on frequency-domain regression method. International Journal of Thermal Sciences, 48 (2009) 2355-2364.
[27] Xiang Qian Li, Youming Chen, J.D. Spitler, D. Fisher. Applicability of calculation methods for conduction transfer function of building constructions. International Journal of Thermal Sciences, 48 (2009) 1441-1451.
[28] B. Delcroix, M. Kummert, A. Daoud, M. Hiller. Improved conduction transfer function coefficients generation in TRNSYS multizone building model. Proceedings of BS2013. 13th Conference of International Building Performance Simulation Association. Chambéry (France) 2667-2674.
[29] C. Luo, B. Moghtaderi, A. Page. Modelling of wall heat transfer using modified conduction transfer function finite volume and complex Fourier analysis methods. Energy and Buildings, 42 (2010) 605-617.
[30] K. Martín, I. Flores, C. Escudero, A. Apaolaza, J.M. Sala. Methodology for the calculation of response factors through experimental tests and validation with simulation. Energy and Buildings, 42 (2010) 461-467.
[31] M. Karmele Urbikain, Morris G. Davies. One-dimensional solutions to Fourier's equation and measures of heat transmission through walls: The role of wall decay times. Building and Environment, 43 (2008) 1433-1445.

[32] M. Karmele Urbikain, Morris G. Davies. Determination of wall decay times by use of a polynomial equation. International Journal of Heat and Mass Transfer, 53 (2010) 3692-3701.

[33] M. Karmele Urbikain, Morris G. Davies. A frequency domain estimation of wall conduction transfer function coefficients. Energy and Buildings, 51 (2012) 191-202.

[34] Jose Manuel Pinazo Ojer, Victor Manuel Soto Francés, Emilio Sarabia Escriva, Laura Soto Frances. Thermal response factors to a 2^{nd} order shaping function for the calculation of the 1D heat conduction in a multi-layered slab. International Journal of Heat and Mass Transfer, 88 (2015) 579-590.

[35] T. Kusuda. Thermal response factors for multilayer structures of various heat conduction systems. ASHRAE Transactions 75 (1) (1969) 246–271.

[36] Youming Chen, Juan Zhou, Jeffrey D. Spitler. Verification for transient heat conduction calculation of multilayer building constructions. Energy and Buildings, 38 (2006) 340-348.

Appendix A. Summary of coefficients for the FDSI method

Table 1: Summary of different coefficients relevant for the FDSI method

<table>
<tr><td colspan="3" rowspan="2">Type of factor</td><td colspan="3" rowspan="2">Integration factors
(pre-calculated factors)</td><td colspan="3">Coefficients that depend on the construction</td></tr>
<tr><td>MFF_X response factors</td><td>MFF_Y response factors</td><td>MFF_Z response factors</td></tr>
<tr><td rowspan="12">For each response factor (asymptotic terms)</td><td rowspan="10">Asymptotic tail terms</td><td rowspan="5">MFF cos</td><td rowspan="2">X</td><td>Outermost layer without thermal inertia</td><td>$KATC1_n = KATC0_n$
$KATC2_n = KATC(+)_n$</td><td>$k_{XTC1} = \frac{\lambda_1}{L_1}$
k_{XTC2}</td><td rowspan="2"></td><td rowspan="2"></td></tr>
<tr><td>Other cases</td><td>$KATC1_n = 0$
$KATC2_n = KATC(+)_n$</td><td>$k_{XTC1} = 0$
k_{XTC2}</td></tr>
<tr><td>Y</td><td colspan="5">No coefficients used (its contribution is negligible)</td></tr>
<tr><td rowspan="2">Z</td><td>Innermost layer without thermal inertia</td><td>$KATC1_n = KATC0_n$
$KATC2_n = KATC(-)_n$</td><td rowspan="2"></td><td rowspan="2"></td><td>$k_{XTC1} = \frac{\lambda_N}{L_N}$
k_{XTC2}</td></tr>
<tr><td>Other cases</td><td>$KATC1_n = 0$
$KATC2_n = KATC(+)_n$</td><td>$k_{XTC1} = 0$
k_{XTC2}</td></tr>
<tr><td rowspan="5">MFF sin</td><td rowspan="2">X</td><td>Outermost layer without thermal inertia</td><td>$KATS1_n = 0$
$KATS2_n = KATS(-)_n$</td><td>$k_{XTS1} = 0$
k_{XTS2}</td><td rowspan="2"></td><td rowspan="2"></td></tr>
<tr><td>Other cases</td><td>$KATS1_n = 0$
$KATS2_n = KATS(+)_n$</td><td>$k_{XTS1} = 0$
k_{XTS2}</td></tr>
<tr><td>Y</td><td colspan="5">No coefficients used (its contribution is negligible)</td></tr>
<tr><td rowspan="2">Z</td><td>Innermost layer without thermal inertia</td><td>$KATS1_n = 0$
$KATS2_n = KATS(-)_n$</td><td rowspan="2"></td><td rowspan="2"></td><td>$k_{ZTS1} = 0$
k_{ZTS2}</td></tr>
<tr><td>Other cases</td><td>$KATS1_n = 0$
$KATS2_n = KATS(+)_n$</td><td>$k_{ZTS1} = 0$
k_{ZTS2}</td></tr>
<tr><td rowspan="2">Asymptotic head terms</td><td>MFF cos</td><td colspan="3">$KAHC1_n$
$KAHC2_n$</td><td>$k_{XHC1} = \frac{1}{\sum_{i=1}^{n} \frac{L_i}{\lambda_i}}$
k_{XHC2}</td><td>$k_{YHC1} = \frac{1}{\sum_{i=1}^{n} \frac{L_i}{\lambda_i}}$
k_{YHC2}</td><td>$k_{ZHC1} = \frac{-1}{\sum_{i=1}^{n} \frac{L_i}{\lambda_i}}$
k_{ZHC2}</td></tr>
<tr><td>MFF sin</td><td colspan="3">$KAHS1_n$
$KAHS2_n = 0$</td><td>k_{XHS1}
$k_{XHS2} = 0$</td><td>k_{YHS1}
$k_{YHS2} = 0$</td><td>k_{ZHS1}
$k_{ZHS2} = 0$</td></tr>
<tr><td rowspan="8">For each interval and response factor (polynomial terms)</td><td rowspan="2">Spline ω^3</td><td>MFF cos</td><td colspan="3">$KPCa_{n,k}$</td><td>$a_{XC(k)}$</td><td>$a_{YC(k)}$</td><td>$a_{ZC(k)}$</td></tr>
<tr><td>MFF sin</td><td colspan="3">$KPSa_{n,k}$</td><td>$a_{XS(k)}$</td><td>$a_{YS(k)}$</td><td>$a_{ZS(k)}$</td></tr>
<tr><td rowspan="2">Spline ω^2</td><td>MFF cos</td><td colspan="3">$KPCb_{n,k}$</td><td>$b_{XC(k)}$</td><td>$b_{YC(k)}$</td><td>$b_{ZC(k)}$</td></tr>
<tr><td>MFF sin</td><td colspan="3">$KPSb_{n,k}$</td><td>$b_{XS(k)}$</td><td>$b_{YS(k)}$</td><td>$b_{ZS(k)}$</td></tr>
<tr><td rowspan="2">Spline ω</td><td>MFF cos</td><td colspan="3">$KPCc_{n,k}$</td><td>$c_{XC(k)}$</td><td>$c_{YC(k)}$</td><td>$c_{ZC(k)}$</td></tr>
<tr><td>MFF sin</td><td colspan="3">$KPSc_{n,k}$</td><td>$c_{XS(k)}$</td><td>$c_{YS(k)}$</td><td>$c_{ZS(k)}$</td></tr>
<tr><td rowspan="2">Spline ω^0</td><td>MFF cos</td><td colspan="3">$KPCd_{n,k}$</td><td>$d_{XC(k)}$</td><td>$d_{YC(k)}$</td><td>$d_{ZC(k)}$</td></tr>
<tr><td>MFF sin</td><td colspan="3">$KPSd_{n,k}$</td><td>$d_{XS(k)}$</td><td>$d_{YS(k)}$</td><td>$d_{ZS(k)}$</td></tr>
</table>

Appendix B. Calculation of the spline coefficients

The coefficients of each cubic polynomial for the MFFs spline interpolation can be easily expressed in terms of the evaluated frequencies (ω_k), the MFF values at those frequencies (y_k) and the corresponding second derivatives ($y_k'' = \sigma_k$), as it is shown in Eqs. B.5.

As ωk and yk are known, the proposed calculation of the spline coefficients is focused on determining the second derivatives. This can be done through the recursive procedure described in Table B.1. For the sake of clarity, the following quantities have been defined:

$$h_k = \omega_{k+1} - \omega_k \qquad 0 < k < n \qquad Eq.B.1a$$

$$r_k = \frac{y_{k+1} - y_k}{\omega_{k+1} - \omega_k} \qquad 0 < k < n \qquad Eq.B.1b$$

Then, φ_k and Γ_k auxiliary terms are obtained in intermediate steps to finally calculate the MFF second derivatives and the spline coefficients.

Table B.1.: Recursive calculation procedure to get the spline coefficients in a global coordinate system

<table>
<tr>
<td>1.- First, φ_k terms are calculated. It requires n-1 iterations, where n is the number of frequency evaluations.

Eqs. B.2.

$$\begin{cases} \varphi_1 = \dfrac{h_2 \cdot (2h_2 - h_1)}{(h_2 - h_1)} & \\ \varphi_k = 2 \cdot (h_{k+1} + h_k) - \dfrac{h_k^2}{\varphi_{k-1}} & 1 < k < (n-1) \\ \varphi_{n-1} = \left(h_{n-2} - \dfrac{h_{n-1}^2}{h_{n-2}}\right) + \dfrac{h_{n-1}}{\varphi_{n-2}} \cdot \left(3h_{n-1} + h_{n-2} + 2\dfrac{h_{n-1}^2}{h_{n-2}}\right) & \end{cases}$$</td>
<td>2.- Once φk terms are stored, we can obtain a sequence of Γk terms, using the recurrence formulae shown below. Again, it requires n-1 iterations.

Eqs. B.3.

$$\begin{cases} \Gamma_1 = \dfrac{6h_2^2}{(h_2^2 - h_1^2)} \cdot (r_2 - r_1) & \\ \Gamma_k = 6 \cdot (r_{k+1} - r_k) - \dfrac{h_k \cdot \Gamma_{k-1}}{\varphi_{k-1}} & 1 < k < (n-1) \\ \Gamma_{n-1} = \dfrac{-6h_{n-1}}{h_{n-2}} \cdot (r_{n-1} - r_{n-2}) + \dfrac{\Gamma_{n-2}}{\varphi_{n-2}}\left(3h_{n-1} + h_{n-2} + 2\dfrac{h_{n-1}^2}{h_{n-2}}\right) & \end{cases}$$</td>
</tr>
<tr>
<td>3.- Given φ_k and Γ_k terms, we can get the second derivatives of the splines σ_k for each evaluation point. Then, note that n σ_k-terms will be needed.

Eqs. B.4.

$$\begin{cases} \sigma_n = \dfrac{\Gamma_{n-1}}{\varphi_{n-1}} & \\ \sigma_k = \dfrac{\Gamma_{k-1} - h_k \cdot \sigma_{k+1}}{\varphi_{k-1}} & 1 < k < n \\ \sigma_1 = \dfrac{\dfrac{-6h_1}{h_2} \cdot (r_2 - r_1) + \left(3h_1 + h_2 + 2\dfrac{h_1^2}{h_2}\right)\sigma_2}{h_2 - \dfrac{h_1^2}{h_2}} & \end{cases}$$</td>
<td>4.- Finally, the coefficients of the splines can be obtained from the list of second derivatives using the following formulae.

Eqs. B.5.

$$a_k = \frac{\sigma_{k+1} - \sigma_k}{6h_k}$$
$$b_k = \frac{\sigma_k \omega_{k+1} - \sigma_{k+1}\omega_k}{2h_k}$$
$$c_k = \frac{\sigma_{k+1}\left(\dfrac{3 \cdot \omega_k^2}{h_k} - h_k\right) - \sigma_k\left(\dfrac{3 \cdot \omega_{k+1}^2}{h_k} - h_k\right)}{6} + \frac{y_{k+1} - y_k}{h_k}$$
$$d_k = \frac{\sigma_k\left(\dfrac{\omega_{k+1}^3}{h_k} - h_k\omega_{k+1}\right) - \sigma_{k+1}\left(\dfrac{\omega_k^3}{h_k} - h_k\omega_k\right)}{6} - \frac{y_{k+1}\omega_k - y_k\omega_{k+1}}{h_k}$$
$0 < k < n$</td>
</tr>
</table>